Effect of Alloy Composition on the Dendrite Arm Spacing of Multicomponent Aluminum Alloys

MARK EASTON, CAMERON DAVIDSON, and DAVID ST JOHN

Predictions of secondary dendrite arm spacing (SDAS) for multicomponent aluminum alloys using a dendrite ripening model are compared with experimental observations. For six of the seven alloys studied, the predicted SDAS was within 20 pct of the measured SDAS. It was found that the final SDAS was dependent upon both the solidification time and the solute profile of the solidifying alloys. It is interesting that while the solidification times and the solute segregation during solidification varied significantly over the range of alloys, these two factors largely canceled each other out so that the predicted SDAS did not vary much between the alloys. The experimental and modeling results show that elements causing high constitutional undercooling near the beginning of solidification, *e.g.*, Ti, which reduces the grain size substantially, have little effect on the SDAS. Instead, it was found that elements that strongly partitioned toward the end of solidification were more effective at restricting SDAS coarsening.

DOI: 10.1007/s11661-010-0183-9

I. INTRODUCTION

OVER the past 60 years, there has been a substantial amount of work on grain refining mechanisms in alloys,[1–3] and the factors affecting the development of grain size are now well established.[4–7] The other feature of the microstructure that is commonly observed in many castings is the secondary dendrite arm spacing (SDAS). A refined SDAS is known to improve many mechanical properties of Al-Si alloys.[8] The SDAS is also known to affect the permeability of semisolid structures during solidification[9–11] and can affect the hot tearing susceptibility of an alloy.[11–13] Hence, knowing how to manipulate or predict the SDAS of an alloy may be useful for optimizing the properties of an alloy or for designing new alloys.

Equiaxed grains tend to grow dendritically for two reasons.[14] First, the thermal profile of an equiaxed grain is such that the grains are at a higher temperature than the surrounding melt. Hence, any perturbation will grow preferentially. Second, the addition of alloying elements leads to the formation of constitutional undercooling in front of the growing grain, which further increases the tendency for perturbations to grow and dendrites to form. The second factor also leads to dendritic growth in columnar growth conditions. In some systems in which the grain size is small enough to satisfy the Mullins–Sekerka stability criterion, spherical growth will occur,[15] *e.g.*, in fine-grained Mg-Zr alloys,[15,16] but in most equiaxed systems, dendritic growth occurs. It should be noted that in some systems, particularly peritectic systems such as Al-Ti, spherical grains may appear to have formed but etching techniques can reveal the dendritic structure formed during solidification of the grains.[17,18]

It is well established that dendrite arms coarsen during solidification.[19,20] Factors governing arm spacing have been proposed to be a combination of competitive growth, coalescence, and ripening,[19] with ripening considered to be the dominant mechanism at low solid fractions.[14,21–23] At higher solid fractions, arm coalescence may become more influential if coarsening continues to occur.[24,25] Experimental data for the secondary SDAS, λ_2, are usually described by the simple empirical equation:

$$\lambda_2 = Kt_f^n \qquad [1]$$

where t_f is the solidification time interval between the liquidus and the solidus, n is between 0.33 and 0.5, and K is a fitting factor. The K is dependent upon the alloy elemental concentration[26,27] and constituents.[28] At long holding times, dendrite arm coarsening leads to spheroidization of the grains.[24,29]

Some effort has been made to model the growth of the dendrites during solidification, primarily based on the assumption that dendrite ripening is the most important coarsening mechanism.[14,22,30,31] Initially, these formulations were confined to binary systems;[14,31] however, more recently, the model for the prediction of dendrite ripening has been extended so

MARK EASTON, Program Manager, CAST Cooperative Research Centre (CRC), is with the Department of Materials Engineering, Monash University, Melbourne 3800, Australia. Contact e-mail: mark.easton@eng.monash.edu.au CAMERON DAVIDSON, Principal Research Scientist, CAST Cooperative Research Centre (CRC), is with the Commonwealth Scientific and Industrial Research Organisation (CSIRO), Division of Process Science and Engineering, Pinjarra Hills, Queensland 4069, Australia. DAVID ST JOHN, Professor, CAST Cooperative Research Centre (CRC), is with the School of Mechanical and Mining Engineering, The University of Queensland, Brisbane, Queensland 4072, Australia.

Manuscript submitted April 20, 2009.
Article published online February 23, 2010

that predictions can be made for multicomponent alloys.[30] According to this model, the SDAS can be predicted by

$$\lambda_2 = 5.5\left(Mt_f\right)^{0.33} \quad [2]$$

where

$$M = \frac{-\Gamma}{\sum_{j=1}^{n} m_j\left(1-k_j\right)\left(c_{f,j}-c_{0,j}\right)/D_j} \cdot \ln\left[\frac{\sum_{j=1}^{n} m_j\left(1-k_j\right)c_{f,j}/D_j}{\sum_{j=1}^{n} m_j\left(1-k_j\right)c_{0,j}/D_j}\right]$$

Γ is the Gibbs–Thompson coefficient, D is the diffusion coefficient, c_f is the final liquid composition (often assumed to be the eutectic composition), m is the liquidus gradient with respect to element j, and k is the partition coefficient for each element j.

Theoretical models that include solute redistribution by convective as well as diffusive means predict an increase in the SDAS as well as n values of 0.5 rather than 0.33.[21,32] The change in n was verified by experiments in which forced convection produced by a magnetic field was found to increase the coarsening rate of the secondary SDAS and also tended to give an n value closer to 0.5 rather than 0.33.[33]

Recently, there has been considerable development of phase field models of solidification,[34–37] including the prediction of the growth of dendrite arms in simple multicomponent systems.[37,38] While these developments are continuing, there is still a need to develop simpler models that are less computationally complex and that provide reasonable predictions of the key microstructural features that can affect material properties.

A different approach, taken by some researchers,[39,40] is to apply mathematical modeling using experimental datasets to determine empirical relationships between the composition and the SDAS. This approach has the advantage of potentially giving more accurate predictions for the alloys used, but has the disadvantage of offering no basis of prediction for alloys with untested elements or element combinations.

Hence, the purpose of this article is to apply the diffusion-based ripening model (Eq. [2]) for predicting the SDAS to complex multicomponent aluminum alloy systems to determine the applicability of the model. Furthermore, the experimental data and model predictions produced by this study enable consideration of the effect of the alloy composition on the final SDAS.

II. EXPERIMENTAL METHODS

This study analyzes the dendrite arm spacings of castings that were the subject of previous studies on grain refinement in which the experimental details are described in full;[4,41,42] hence, a briefer description is given here.

Seven wrought alloys (1050, 2014, 3003, 5083, 6060, 6061, and 6082) (Table I) were melted in 1- to 2-kg batches in a resistance furnace. Additions of 0.005, 0.01, and 0.02 wt pct TiB_2 *via* an Al-3Ti-1B grain refiner master alloy were made along with three different additions of solute Ti up to 0.05 wt pct. These alloys were solidified in a preheated graphite crucible in which the presolidification cooling rate was measured to be approximately 1 K/s. The dimensions of the crucible were a 50-mm outer diameter, a 5-mm height, and a wall thickness of 10 mm.[43] Alloys 1050, 5083, 6060, and 6061 were prepared with 0.005 pct TiB_2 at additions of Ti up to 0.05 pct, and were cast at cooling rates of 0.3 K/s, 4 K/s, and 15 K/s. These various cooling rates were measured in samples in which the crucible was packed in Fiberfrax,* cooled with forced air, and cooled with water spray, respectively. These "cooling rates" were determined in the fully liquid state at temperatures just above the liquidus. Because the cooling rate is controlled in these experiments by a rate of energy extraction that decreases monotonically with decreasing temperature, the cooling rates during solidification will be significantly lower. In particular, it should be noted that in some of the previous literature,[44] an "average cooling rate" between the liquidus and solidus was used. That form of cooling rate is not simply proportional to the cooling rate before solidification, because it also includes a material-dependent component related to the rate of latent heat release with temperature.

*Fiberfrax is a registered trademark of Unifrax, Melbourne, Australia.

Metallographic samples were prepared as described previously.[4,41,42] After polishing, the samples were anodized in Barker's reagent and viewed optically under polarized light. The dendrite arm spacing was measured by finding a number of adjacent dendrite arms from one primary dendrite arm and measuring the distance between the dendrite centers. Wherever possible, at least two fields were analyzed for each measurement, with

Table I. Average Alloy Compositions for Alloys as Measured by Inductively Coupled Plasma-Atomic Emission Spectroscopy; These Compositions Were Used for SDAS Modeling

Alloy	Si (Wt Pct)	Fe (Wt Pct)	Mg (Wt Pct)	Cr (Wt Pct)	Mn (Wt Pct)	Cu (Wt Pct)
1050	0.2	0.27	<0.01	<0.01	<0.01	<0.01
2014	1.09	0.51	0.45	<0.01	0.45	4.78
3003	0.55	0.58	0.01	<0.01	1.37	0.12
5083	0.35	0.29	4.24	0.17	0.86	<0.01
6060	0.54	0.12	0.31	<0.01	<0.01	<0.01
6061	0.83	0.05	0.73	<0.01	<0.01	0.21
6082	1.09	0.04	0.60	<0.01	0.46	<0.01

approximately 50 secondary dendrite arms from multiple primary dendrite arms being counted in each field.

III. EXPERIMENTAL RESULTS

The change in dendrite morphology as the grain size is reduced is very important to the measurement of the SDAS. With no grain refiner addition, the grains were large and dendritic and could be either columnar or equiaxed (Figures 1(a) and (b)). As the grains were refined, they changed to a fully equiaxed dendritic grain structure (Figures 1(c) and (d)). Further grain refiner addition led to a more globular grain structure (Figures 1(e) and (f)), as noted previously.[45] The SDAS is easily measured when the grains are large, but as the grain size decreases, it is more difficult or impossible to measure. For spherical grain structures, such as Figure 1(e), it is impossible to obtain a meaningful measurement of the SDAS.

It is apparent from Figure 2 that once an equiaxed grain structure was obtained, the addition of Ti made no systematic difference to the SDAS for these alloys. It was also found that Al3Ti1B additions made no difference to the SDAS; they only reduced the grain size. For this reason, the data for a particular alloy at a

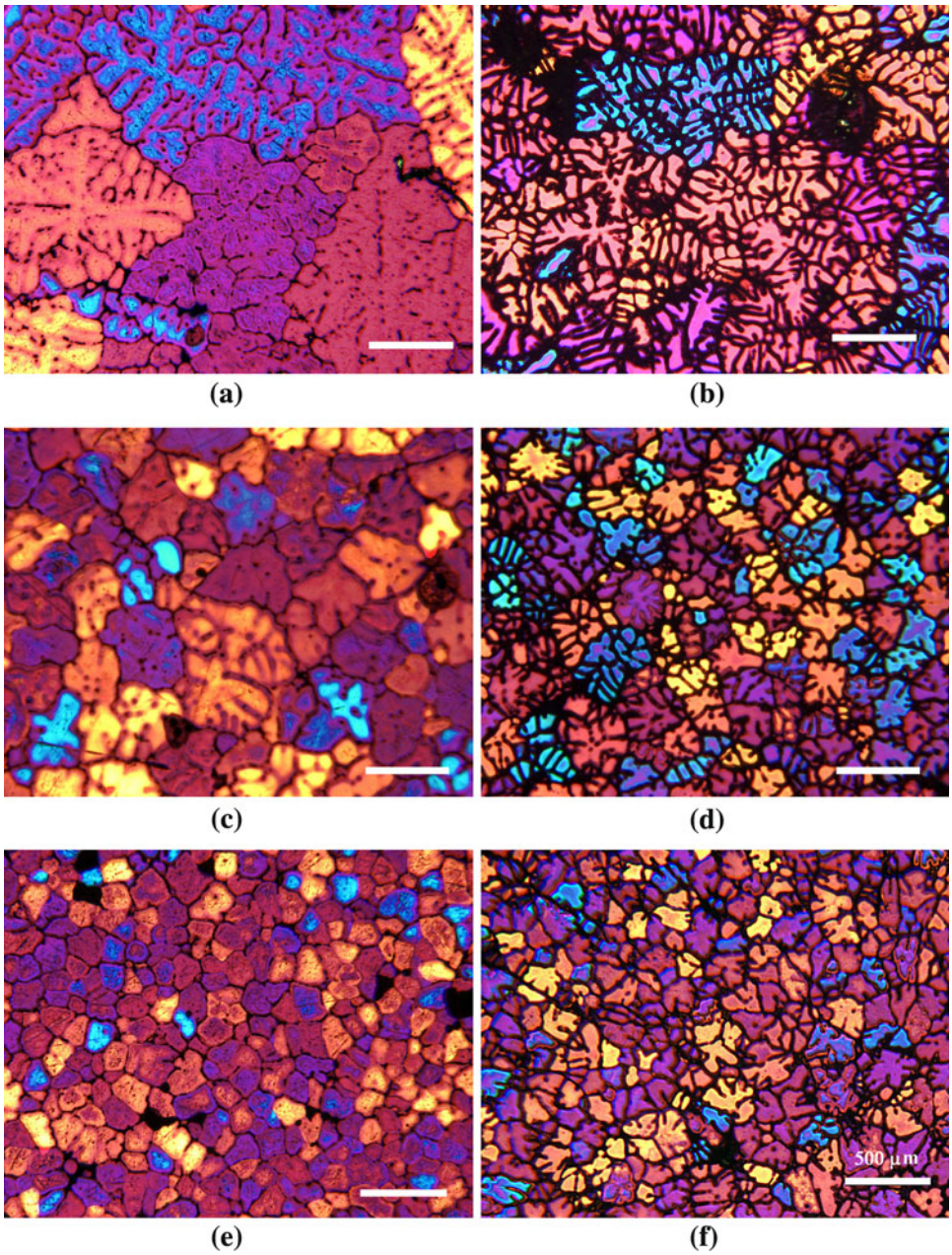

Fig. 1—Optical micrographs using polarized light of (*a*) 6061 and (*b*) 2014 without grain refiner additions; (*c*) 6061 and (*d*) 2014 grain refined with a 0.01 pct TiB_2 as Al3Ti1B addition; and (*e*) 6061 and (*f*) 2014 with a 0.02TiB_2 as Al3Ti1B addition plus approximately 0.05 pct Ti as solute. All samples were cooled at 1 K/s. The scale bar in each of the micrographs is 500 μm.

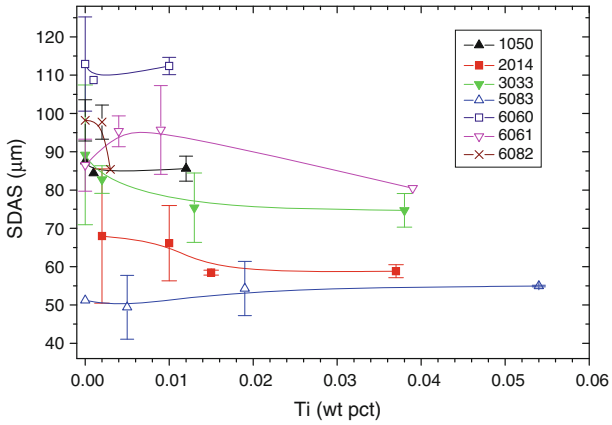

Fig. 2—Measured SDAS as Ti contents increase for each of the alloys at a cooling rate of 1 K/s and a TiB_2 concentration of 0.005 wt pct. A useful measurement of SDAS at Ti additions of 0.05 Ti was difficult to obtain in some alloys because these alloys were typically globular rather than dendritic.

Table II. Measured SDAS for Each of the Alloys Solidified at 1 K/s

Alloy	$\lambda_{2,\text{meas}}$ (μm)	Standard Deviation (μm)
1050	85.7	2.3
2014	62.3	8.1
3003	83.9	12.4
5083	51.4	5.1
6060	111.3	6.5
6061	90.1	7.5
6082	91.4	9.3

particular cooling rate were grouped and averaged to produce the data presented in Table II. One of the advantages of this approach is that the difficulties with measuring the SDAS in globular and spherical structures, *e.g.*, for the 0.05Ti samples for some alloys, do not influence the results, because a representative SDAS can be obtained using the less refined castings for a particular cooling rate.

Figure 3(a) shows the influence of the cooling rate just above the liquidus on the SDAS. The values are plotted against the cooling rate at the liquidus because that is an unambiguous and independent experimental parameter. These plots have been fitted to Eq. [1], in which the cooling rate substituted for $1/t_f$. The coefficients are presented in Table III, with the n values falling within the expected range of 0.33 to 0.5.[14] Of the four alloys tested, alloy 5083 consistently had the finest SDAS while the others had similar values of SDAS. The similarity in the SDASs is to some extent a coincidence, because the alloys have different freezing ranges and therefore different t_f values for a given cooling rate, which is illustrated in Figure 3(b), in which the SDAS is plotted against t_f. From a theoretical perspective, it would be preferable to relate the SDAS to t_f, however t_f is dependent both on material characteristics and on experimental heat flow conditions. The consequences of relating SDAS to the presolidification cooling rate (heat extraction rate) or t_f are discussed in more detail in Section IV–A.

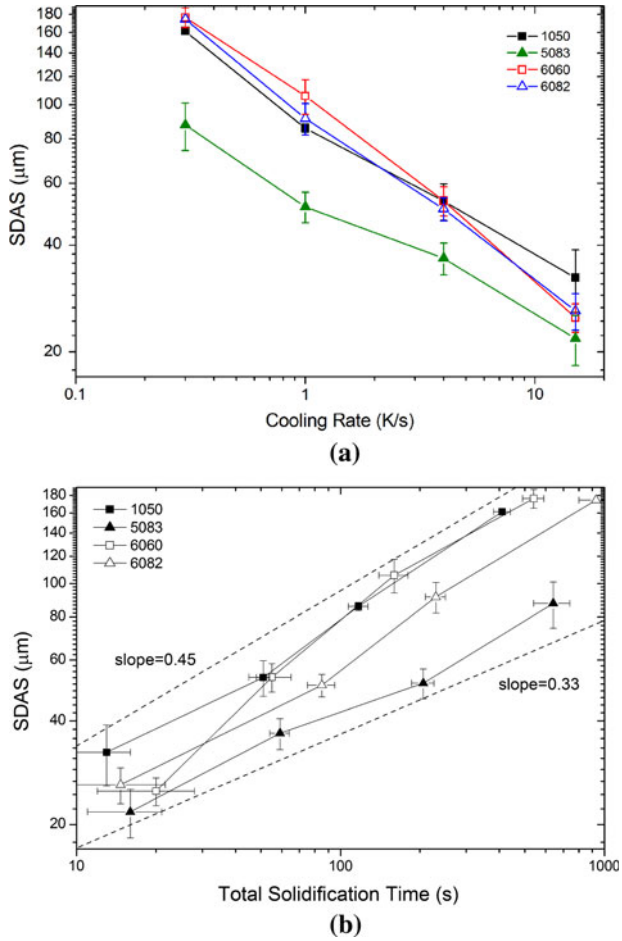

Fig. 3—Plots of the SDAS of the each of the alloys plotted against (*a*) the cooling rate just above the liquidus and (*b*) the total solidification time (as determined from cooling curves). Dashed lines are arbitrary lines illustrating the effect of the exponent in Eq. [1]. Extreme t_f values for alloy 5083 were not determined and were therefore estimated from scaling rules.

Table III. Data for Lines of Best Fit of Data Presented in Figure 3(a) to the equation: log(SDAS) = log(K) – n log(Cooling Rate)

Alloy	K (μm)	n	R^2
1050	91.3	0.40	0.98
5083	55.9	0.34	0.99
6060	101.3	0.50	0.996
6082	95.8	0.48	0.998

It was also observed that as the cooling rate increased, a finer and more dendritic grain morphology was obtained in the alloys studied (Figure 4), indicating that the SDAS decreased with the increasing cooling rate more rapidly than the grain size.[12]

IV. MODEL PREDICTIONS OF THE SDAS

A. *Determination of Solidification Time*

To be able to use Eq. [2] to predict the SDAS, a number of factors need to be determined. One of the

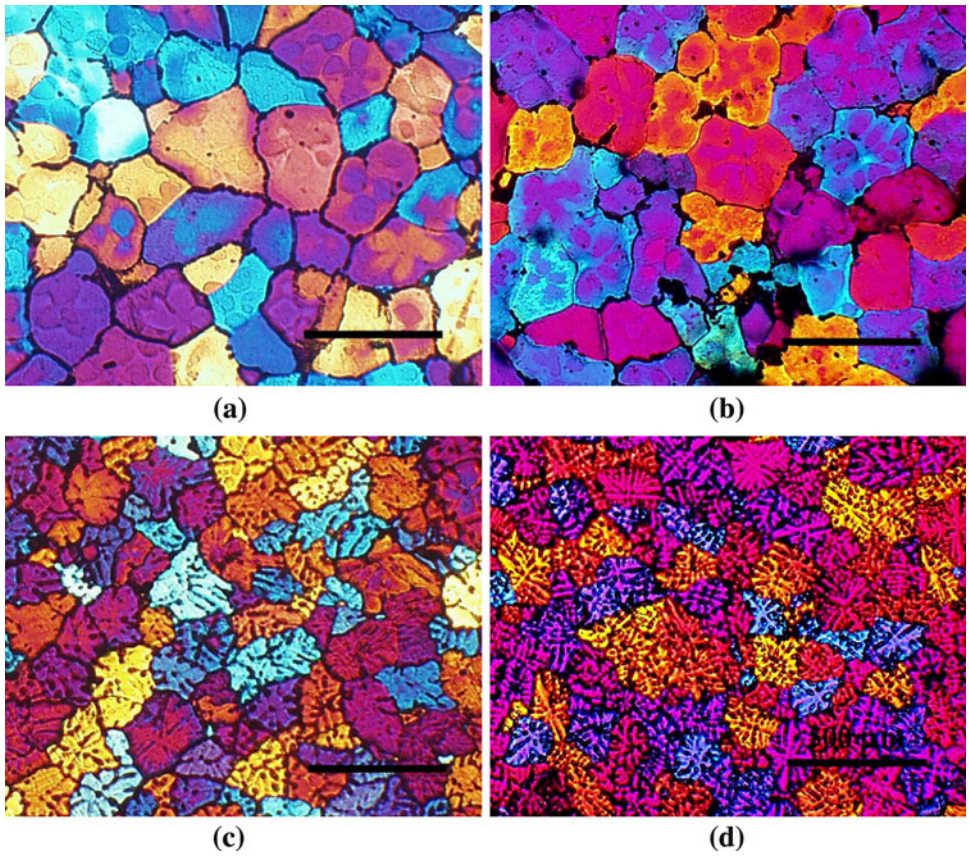

Fig. 4—Alloys (*a*) 1050 and (*b*) 5083 with 0.005TiB_2 as Al3Ti1B addition and 0.05 Ti as solute cooled at 0.3 K/s. The same alloys, (*c*) and (*d*), respectively, cooled at 15 K/s. The scale bar in each of the micrographs is 500 μm.

most important factors is the solidification time t_f, which is dependent upon the alloy composition and the heat extraction rate. Simple heat flow considerations can provide a predictive approach to calculating t_f. The cooling rate is related to the heat extracted from the melt and the latent heat evolved during solidification by the equation:

$$\dot{T} = \frac{-q_e A}{m_c \cdot C_{p,c} + m_m \cdot C_{p,m} - m_m \Delta h_f \left(\frac{df_s}{dT}\right)} \qquad [3]$$

where $\dot{T}$ is the cooling rate at a particular point in time, q_e is the external heat flux, A is the surface area of the crucible, m_m is the mass of the melt, f_s is the fraction solid, Δh_f is the latent heat of fusion, and C_p is the specific heat capacity.[14] The subscripts c and m refer to the crucible and metal, respectively. Parameters q_e, $C_{p,c}$, and f_s are assumed to be temperature dependent during solidification, while the remainder are constant. Equation [3] was converted to a differential form, and Δt_f was calculated at 0.5 K intervals and numerically integrated to give predictions of t_f as a function of the final fraction solid.

The variation in q_e with temperature was determined by experimental measurements on a block of graphite of the same external dimensions as the crucible for the case in which the presolidification cooling rate was 1 K/s. The calculated heat flux was fit to the following quadratic equation over the temperature range 573 to 973 K (300 to 700 °C):

$$q_e = -5830 + 28 \times T + 0.073 \times T^2 \qquad [4]$$

where T is in degrees Celsius and q_e is in watts per square meters. The value of R^2 for the fit was 0.996. The predictions of q_e were scaled proportionally for the other cooling rates. The validity of the prediction was verified for the current experimental conditions, although there was significantly higher variability (±30 pct) at the highest cooling rate condition, both from one curve to the next and even within a single sample.

To estimate the solidification time t_f, additional factors need to be defined in Eq. [3]: Δh_f is assumed to be 390 kJ/kg and C_p is assumed to be 1050 J/kg·K.[14] The C_p for graphite was taken from NIST equations.[46] By using these values for aluminum, the assumption is made that only solid Al is being precipitated, which is reasonable because it is by far the dominant phase, especially early in solidification. A somewhat more precise technique would be to use enthalpy tables directly from thermodynamic calculations, but this was not done in this case because the difference was assumed to be insignificant for these relatively dilute alloys.

In a simple binary alloy, only one solid phase grows over the temperature interval from the liquidus to the solidus, or just above the solidus if there is a final eutectic. However, in multicomponent alloys, the reactions that occur during solidification are often complicated, with secondary phases usually solidifying well above the solidus. The precipitation of phases early in the solidification sequence could have two consequences for a ripening model. First, the minor phases would appear to delineate dendrites independent of any ripening of the neighboring dendrite arms. Second, the formation of the new phase will locally alter the solute gradients in the liquid, which might disrupt the ripening process. For purposes of evaluating the model, it was assumed that for each alloy system, there is a key solidification reaction that effectively determines the final SDAS and that negligible ripening occurs at lower temperatures after the key reaction is complete.

The data for the fraction solid at various temperatures $f_s(T)$ were obtained from ThermoCalc** using the ThermoTech TT-Alv6 database (Thermotech Ltd., Surrey Tech. Centre, Guildford, UK) (Figure 5) using the nonequilibrium Scheil–Gulliver module, which is generally used for modeling solidification processes. It is seen that the alloys studied exhibit a wide range of solidification paths. One of the considerations for choosing the key reaction that defines the final SDAS was that it occurs later in the solidification sequence, *i.e.*, when there is less liquid for solute transport. Another consideration was that the reaction is related to the prevalent SDAS boundary phase (eutectic or precipitates) in each of the alloys. The key reactions were identified through the authors' own investigations, *e.g.*, β AlFeSi in the 6000-series alloys or by using the observations of other researchers who have studied those alloys.[28] Obviously, there is some discretion as to which reaction was chosen, particularly in alloys in which intermetallics form almost throughout the whole of solidification, *e.g.*, in alloys 3003 and 5083. However, to some extent, the reaction chosen toward the end of the solidification process does not have a very significant effect on the estimated SDAS, as will be shown later, because most coarsening takes place early in solidification.

**ThermoCalc is a trademark of Thermo-Calc Software AB, Stockholm, Sweden.

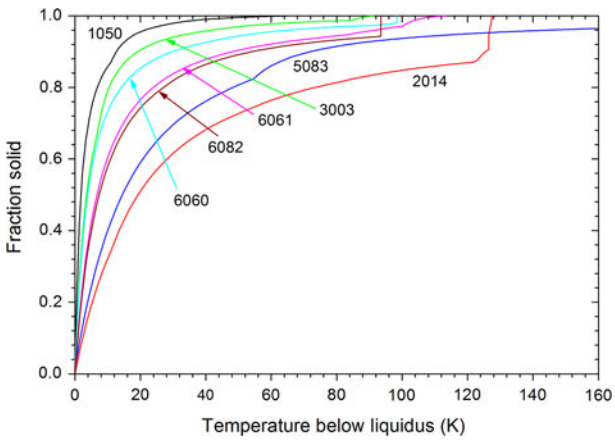

Fig. 5—Thermo-Calc predictions of the development of fraction solid assuming Scheil–Gulliver solidification.

B. *Inputs to the Modeling*

To obtain SDAS predictions from Eq. [2], input data for a number of factors are required. The Gibbs–Thompson coefficient (Γ) was assumed to be 2×10^{-7} K·m.[47] Table IV lists the liquidus gradient (m) and the partition coefficient (k), and compares values from binary alloys with those derived from thermodynamic calculations specific to each alloy.

It is difficult to obtain an accurate value of the diffusion coefficient in the liquid, and often a value of 3×10^{-9} m^2/s is assumed across all alloys, *e.g.*, References 21,31, and 48. Recently, expressions for the diffusion coefficients of a range of elements have been determined by considering previously published experimental data,[49] and the factors determining the diffusion coefficients are given in Table V. The diffusion coefficient for each of the elements in each alloy was calculated as the average over each temperature range.

Table IV. The m and k Values for a Variety of Elements in Binary Aluminum Alloys;[57] Data for Al-Ti Was Obtained from Reference 58; Also Included Are the Ranges of Values at the Liquidus Temperatures Determined by Thermodynamic Modeling for the Alloys Studied (Including Only Those Elements Present in Significant Quantities)

	Binary Alloy		Predicted (Multicomponent) Ranges	
Element	k	m	k	m
Ti	7.33	30	10	34
Si	0.11	−6.6	0.09 to 0.11	−4.6 to −6.2
Cr	2.0	3.5	3.6	0.15
Mg	0.51	−6.2	0.3 to 0.36	−4.5 to −5.1
Fe	0.02	−3.0	0.02 to 0.03	−1.6 to −4.3
Cu	0.17	−3.4	0.10	−2.6 to −3.0
Mn	0.94	−1.6	0.67 to 0.9	+0.5 to −2

Table V. Factors for Arrhenius Equation, $D = D_0 e^{-\frac{Q_a}{RT}}$, for Diffusivity of Elements in Liquid Al[49]

Element	D_0 (m^2/s)	Q_a (kJ/mole)
Ti	4.29×10^{-7}	36.3
Cr	2.53×10^{-7}	32.8
Mn	1.93×10^{-7}	31
Fe	2.34×10^{-7}	35
Cu	1.06×10^{-7}	24
Zn	5.12×10^{-8}	22.2
Mg	9.90×10^{-5}	71.6
Si	1.34×10^{-7}	30

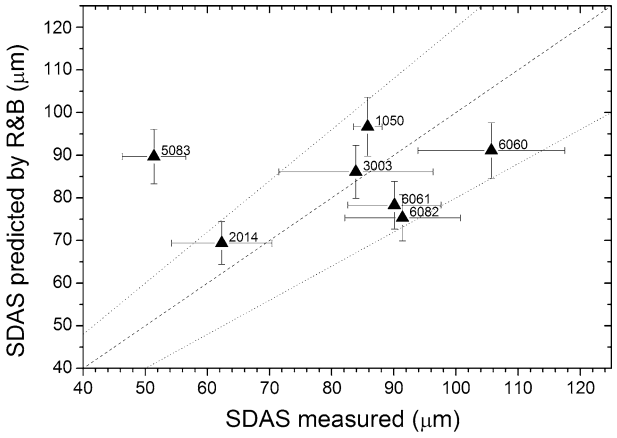

Fig. 6—Predicted SDAS from Rappaz and Boettinger model against the measured values at 1 K/s cooling rate. Error bars on the prediction are derived from the observed deviations from the nominal cooling rate. Dashed line is a perfect match, while dotted lines show ±20 pct deviation.

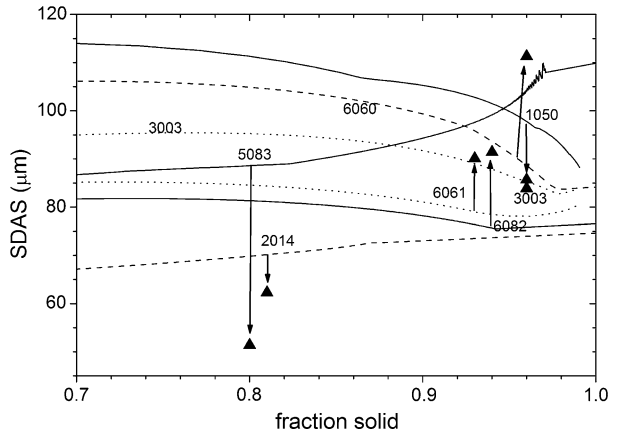

Fig. 7—Plot of SDAS predicted for each alloy as a function of the fraction solid that determines dendrite size. Presolidification cooling rate of 1 K/s was assumed. Curves are labeled with the alloy, and each arrow points from the prediction line for each alloy to its experimentally measured value.

C. *Model Results*

The SDAS values determined using the considerations mentioned here are shown in Figure 6. It is seen that the predictions are within 20 pct of the measured SDAS for all alloys except 5083, in which the SDAS was predicted to be 70 pct above the observed SDAS.

By using temperature-dependent tables of the various parameters, Eqs. [2] through [4] can be used to estimate the SDAS as a function of the fraction solid that is assumed to mark the end of microstructural change. The values of $c_{f,j}$ used in each calculation are given by the liquid concentration at the end point and for other parameters, the mean value between the start and end point is used. These predictions are shown in Figure 7 together with the measured values plotted at the fraction solid assumed to mark the fixing of the SDAS.

Note that these curves are not predicting the evolution of coarsening during solidification; they are not an integration over the solidification interval but are simply calculating values based on assumed end points. Even so, the calculations provide an idea of how the SDAS may coarsen during solidification. It indicates that by halfway through the solidification process, the SDAS of most of the alloys has coarsened to at least 80 pct of the value predicted at the end of solidification. However, calculations for many of the alloys appear to arrive at the physically unrealistic conclusion that the SDAS would reduce at high solid fractions, having maximized earlier in the solidification process. The primary reason for the predicted reduction in the SDAS is thought to be due to these materials not conforming to a key assumption behind the derivation of Eq. [2], namely, that the liquid composition of each element varies linearly with time.[30] Figure 8 shows that in no case is this condition met, with most elements showing a monotonically increasing rate of concentration increase while some element concentrations decrease in the liquid as certain precipitation reactions occur, which in turn leads to a reduction in the SDAS predicted. While the liquid composition may decrease in some alloys due to the precipitation of various phases, this will not lead to a reduction in the SDAS.

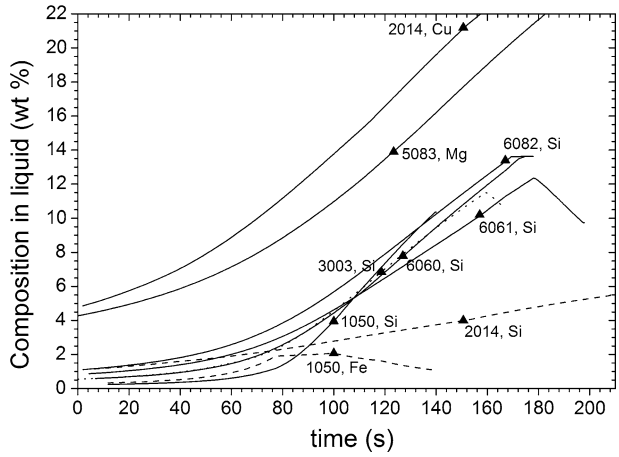

Fig. 8—Variation in liquid composition with time during solidification. Only the elements with the strongest influence in each alloy have been plotted: the most important element for each alloy is shown with a solid line; other significant elements are shown with dashed lines. Markers indicate the time (solid fraction) at which the SDAS calculations in Fig. 6 were made.

Alloy 5083 shows an apparently contrary trend of increasing sensitivity to the chosen end point past 80 pct solid (Figure 7). This is a distortion brought about by the use of the fraction solid as the *X*-axis: the final 20 pct of solidification in this alloy is calculated to occur over a temperature range that exceeds the entire solidification range of any of the other alloys.

V. DISCUSSION

A. *Measurement and Model Accuracy*

The model was able to give a surprisingly accurate prediction of the SDAS for the alloys chosen (Figure 6),

especially when it is considered that the model has no adjustable parameters and that a number of the assumptions underlying the model were not met in these materials. Six of the seven alloys fell within 20 pct of the measured values (Figure 6), which is approximately 2 standard deviations from the measured mean (Table II). Despite the excellent match to the average SDAS, there was not a good prediction of the relative variation in the SDAS on the alloy composition, mainly because the predictions for all the alloys were relatively similar. The reason for the small variation in the predicted SDAS of the alloys was that the alloys with the longer solidification times (Figure 3(b)) tended to have much smaller M values due to a greater solute effect. Hence, the two major contributions to the dendrite arm spacing tended to vary in opposite directions, cancelling each other out.

One source of error in predicting the time-temperature dependency is the reduction in the heat extraction rate when the air gap forms between the crucible and the nearly solid alloy.[50] Fortunately, it is likely that the scale of the SDAS is already determined by this time. Furthermore, errors in the prediction of the solidification path by thermodynamic modeling are likely to occur for two reasons: first, the Scheil–Gulliver equation does not incorporate back diffusion and so overestimates both the liquid fraction at a given temperature and the amount of intermetallic phase formed,[51] and second, peritectic type reactions are not considered, which may lead to errors in the solute balance in the liquid. Because the SDAS is related to the M and t_f values through a cube-root relationship, large changes in either of these values lead to relatively small changes in the predicted SDAS. The cube-root relationship means that the prediction is relatively insensitive to errors in the input values, *e.g.*, a factor of 2 error in the solidification time will change the predicted SDAS by only 26 pct.

Alloy 5083 showed the poorest agreement between the prediction and the measurement in which the predicted SDAS was 70 pct higher than measured. It is also the alloy for which the largest fraction of intermetallics is formed early in solidification, even before the formation of the α Al. It is possible that the formation of intermetallics early in the solidification process restricts the coarsening processes, as has been reported in the solidification of composites,[52] leading to an overestimate of the SDAS by the model. Furthermore, these intermetallics, when formed between the dendrite arms, will demarcate dendrites at lower solid fractions than in other alloys. However, a difficulty with this explanation is that alloy 3003 is also predicted to produce intermetallics early in solidification, although not as much, but it gave the best agreement between prediction and measurement. A second unusual feature of the 5083 alloy was that it had the greatest deviation between prediction and measurement for the total solidification time, as determined by the cooling curve. The experiments suggest it had a much shorter solidification interval than predicted, and no final eutectic was detected. There is no obvious reason that this alloy should deviate much further from the Scheil–Gulliver predictions than the other alloys.

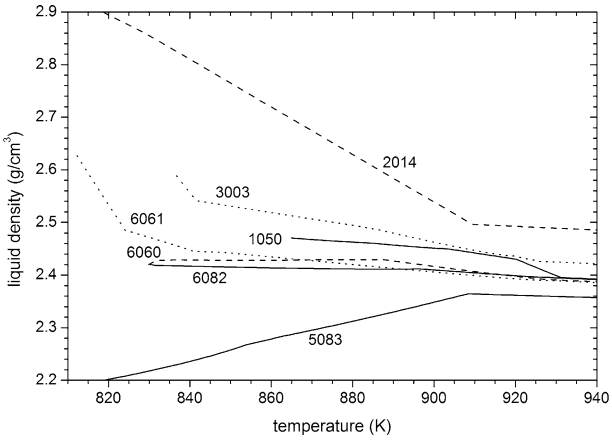

Fig. 9—Prediction of liquid phase density for each alloy during Scheil–Gulliver simulations.

The different relative sensitivity to cooling rate, as revealed by the power n in Table III, could indicate that alloys 6060 and 6082 were strongly influenced by convection while alloy 1050 was slightly influenced and 5083 was not influenced at all. Because convection increases the SDAS, it would be expected that convection would lead to underprediction of the SDAS for 6000-series alloys. In fact, the 6000 alloys were found to be the only ones in which the predicted SDAS was lower than the measured value.

A driving force for thermosolutal convection is likely to be density changes in the liquid during solidification. The JMatPro software (Sente Software Ltd, Surrey Tech. Centre, Guildford, UK) provides the facility to model solid and liquid densities during Scheil–Gulliver simulations[53,54] (Figure 9). A simple qualitative interpretation of Figure 9 might suggest that a tendency to thermosolutal convection would increase as the slope deviated from zero, either positively or negatively, suggesting that alloys 2014 and 5083 would be the most affected. This observation does not agree with the interpretation of the observed n values. It is also possible that the presence of intermetallics during solidification may upset convective processes. Hence, it appears that simple estimates such are this are apparently inadequate to predict changes in the n value, or there are more factors involved in the cooling rate sensitivity than just convection.

It has already been noted (Figure 7) that the model calculations appear to give a physically unrealistic prediction for some alloys in which the SDAS predicted at higher solid fractions is lower than at a lower solid fraction. This behavior may be related to the degree to which the alloy deviates from the assumption of the liquid composition varying linearly with time: the greater the deviation, the larger the anomalous effect.

The deviations may be more pronounced in the leaner alloys, in which deviations from the assumptions are stronger. A simple measure of "leanness" in a complex alloy is the amount of solid formed within a set temperature below the liquidus. In fact, it may be this leanness, with its larger range of df_s/dT over the solidification interval, that translates to a larger range of dc_i/dt, at least for these alloys. Other nonlinearities,

particularly of the diffusion coefficients, may also play a part. When the solidification path reaches a reaction such as a monovariant eutectic, the value of m then becomes rather ambiguous. Values for m determined by thermodynamic modeling were found to be relatively constant for the duration of single-phase alpha dendrite growth, and so these same values were used in the multiphase regions.

Overall, it appears that the Rappaz and Boettinger model includes the most important factors that affect the SDAS in alloys, although the precipitation of intermetallic phases early in the solidification sequence may lead to a reduction in the SDAS compared to the predictions. Convective flow during solidification may have had a minor affect on the SDAS, but it could not be substantiated. Likewise, deviations from the model assumption that the liquid composition increases linearly with time appears to lead to errors in the calculations, but these are relatively minor. However, the model is unable to consistently predict trends between the changing alloys. Given the uncertainty of the currently known values of the parameters used in the model and the uncertainty in the experimental measurements, it is not clear whether this poor correlation represents a limitation of the model or of the data.

B. *Manipulating the SDAS*

Because the SDAS can affect alloy properties and defect size, it is desirable to know whether the SDAS can be manipulated. It is well known that the SDAS can be reduced substantially by increasing the cooling rate (Eq. [1]) and consequentially decreasing the solidification time. However, this study has confirmed that the alloy composition can also affect the SDAS substantially and could be another route to manipulating the SDAS of an alloy.

By considering Eq. [2], it can be seen that the compositional factor that most affects the SDAS is $Q = \sum_j m_j c_j (k_j - 1)$. In fact, the value of M in Eq. [2] can be rendered as

$$M = \frac{-\Gamma}{\sum_{j=1}^{n} (Q_{0,j} - Q_{f,j})/D_j} \cdot \ln \left[\frac{\sum_{j=1}^{n} -Q_{f,j}/D_j}{\sum_{j=1}^{n} -Q_{0,j}/D_j} \right] \qquad [5]$$

where Q_0 is the value for the initial alloy concentration and Q_f is the value for the composition of the liquid at the temperature at which the SDAS is determined, usually due to a final eutectic reaction. The value Q_0 has been shown to be very important in grain refinement,[5,7,55,56] in which it is denoted as Q[4,5,7] or GRF.[56]

It is not surprising that similar factors are involved in prediction both of the grain refinement and of the SDAS, because both are related to the development of constitutional undercooling. From Eq. [5], it is seen that not only is the initial rate of development of constitutional undercooling, Q_0, important, but so is the development of constitutional undercooling at the end of solidification, Q_f.

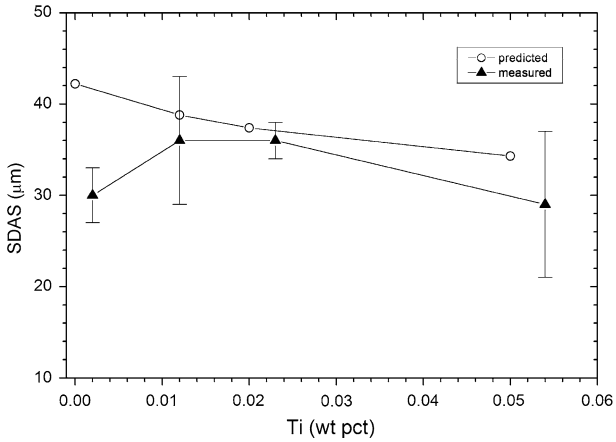

Fig. 10—Plot of the SDAS against the solute Ti content for alloy 1050 at a cooling rate of 15 K/s compared with the predictions of the model.

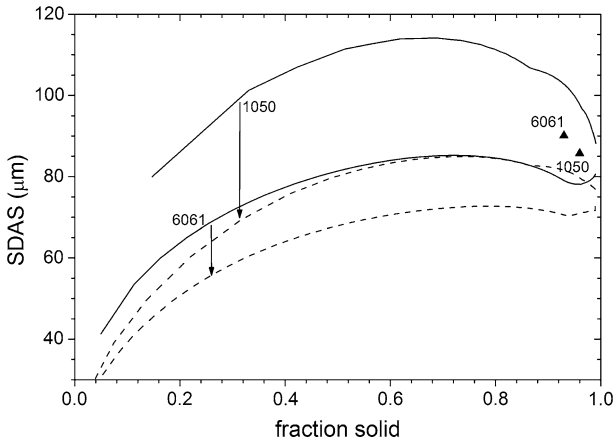

Fig. 11—SDAS during solidification at a presolidification cooling rate of 1 K/s for alloys 1050 and 6061 with (dotted line) and without (solid line) the addition of 0.05 Ti as solute. Arrows indicate the calculated shifts due to the Ti addition.

Solute Ti has been shown to be very effective at grain refining aluminum alloys. In lean alloys such as 1050, the addition of solute Ti can reduce the grain size by up to 80 pct,[4] because the relative effect on Q_0 per unit mass for solute Ti is 30 to 40 times that of other typical alloy additions. A comparison is made in Figure 10 between the model predictions and the measured SDAS for the highest cooling rate of 15 K/s for the addition of Ti to alloy 1050. This cooling rate was chosen because the grains are more dendritic (Figure 4(c)) and the SDAS can be measured for a Ti content of 0.05 pct, which could not be done at lower cooling rates because of the globular grain structure (Figure 4(a)). It is seen that the prediction is close to the experimental data, but the predicted reduction in SDAS is only approximately 20 pct, which is too small to observe conclusively experimentally, and this is the reason that the experimental results (Figure 2) appear to show no observable change in SDAS with Ti content.

To further investigate the role of Ti and its effect on the SDAS, a comparison was made between alloy 1050 and alloy 6061 at 0 and 0.05 Ti contents for a cooling

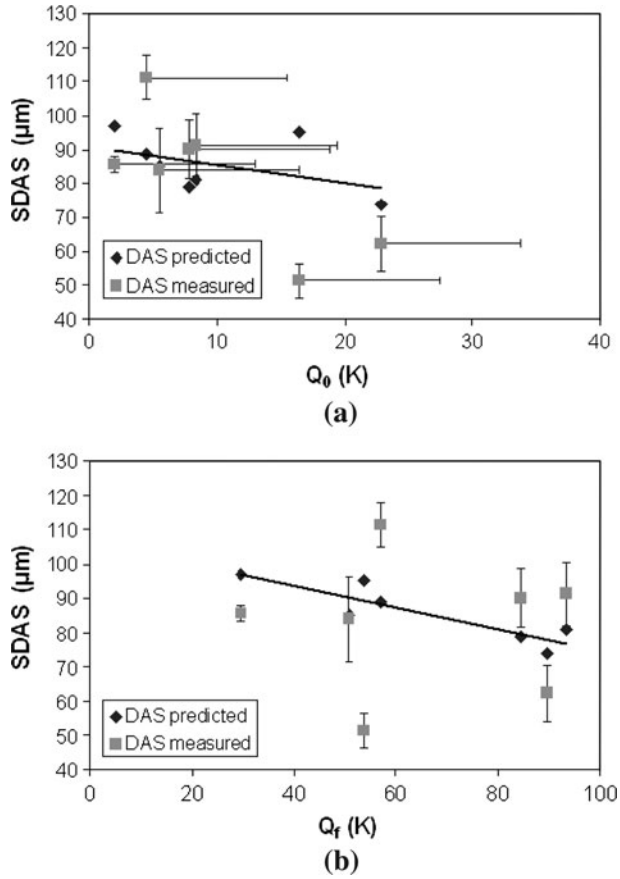

Fig. 12—Plots of (*a*) Q_0 and (*b*) Q_f against the predicted and measured values of SDAS in this study. Extended *x* error bar in (a) shows the variation in Q_0 caused by the addition of Ti. The Ti is removed from the liquid before the end of solidification and has no effect on Q_f. Line of best fit for the predicted values in (a) was SDAS, $\lambda_2 = -0.53 \times Q_0 + 91$, $R^2 = 0.21$, while in (b) it was $\lambda_2 = -0.35 \times Q_f + 105$, $R^2 = 0.81$.

rate of 1 K/s (Figure 11). By plotting the SDAS against the fraction solid, it is observed that the addition of Ti restricts the coarsening at low fraction solids but not at higher fraction solids, because the Ti has already been removed from the liquid due to its being a peritectic element.[17] The effect is greater in the leaner 1050 alloy, in which the SDAS is predicted to be reduced by approximately 20 pct, than in alloy 6061, in which only a 10 pct reduction is predicted.

The reason for the relatively small effect of the Ti additions on the SDAS is that the SDAS is most dependent upon the liquid becoming highly enriched by eutectic solute elements near the end of solidification, *i.e.*, Q_f is very high. Enrichment of the solute toward the end of solidification is more effective at restricting the coarsening of SDAS than the initial rate of undercooling development, Q_0, in which the Ti addition has a much greater effect. Figure 12(a) shows that there is a very poor correlation between Q_0 and the measured or predicted SDAS values, particularly if the addition of Ti is considered; the Ti changes Q_0 substantially but was found to have little effect on the SDAS. However, Figure 12(b) shows a good correlation between Q_f and the predicted SDAS values (R^2 = ~0.8). In this case, Q_f was determined by using the predicted solute content and k at the point in the solidification at which SDAS was assumed to be determined. It can also be seen that except for the point for alloy 5083, which has already been identified as one in which the observations are significantly different from the model, the experimental results show a similar trend. Hence, it appears that Q_f accounts for most of the predicted compositional dependence in the present calculations. More precise evaluation may require better data (such as composition-dependent values for Γ) or better evaluation of the nonlinear rate of change of liquid compositions. This finding is worthy of further research over a broad range of alloys, in order to assess the importance of Q_f and its potential as a predictive parameter of the effect of the alloy composition on SDAS.

VI. CONCLUSIONS

The SDAS was found to be influenced by the alloy composition but not by grain refinement. Hence, grain refinement changes only the grain morphology, leaving the SDAS unchanged. In general, there was good agreement (within 20 pct) between the predictions of an SDAS coarsening model, which used no adjustable parameters, and experimental measurements of SDAS. In the one case of poor agreement, the model overestimated the value of the SDAS in alloy 5083 by approximately 70 pct. It is proposed that the overestimate is due to the early precipitation of intermetallics in this system, which then masks the effects of further coarsening.

The n values also varied between alloys and it was investigated whether this could be related to different alloys having lesser or greater susceptibility to solutal convective flow. No correlations were identified that could aid the prediction of this parameter.

Two major factors were identified that may limit the use of predictions in complex alloy systems such as those used here. One is the assumption of linear trends of liquid concentration with time, which is rarely fulfilled, and the other is the solidification of minor intermetallic phases in the interdendritic spaces creating a condition in which the coarsening end point is difficult to predict and may, in fact, be indistinct.

The Rappaz and Boettinger model can be expressed in terms of the parameter $Q = \sum_j m_j c_j (k_j - 1)$. It incorporates Q_0 at the beginning of solidification and Q_f for the point in solidification at which the SDAS is established. Large changes in Q_0, which are correlated with large changes in grain refinement, were found to have little effect on either the predicted or the measured SDAS. However, there is a strong correlation between Q_f and the predicted SDAS, suggesting that Q_f is the dominant parameter in the current evaluation.

ACKNOWLEDGMENT

The CAST CRC was established under and is supported in part by the Australian Government's Cooperative Research Centres scheme.

REFERENCES

1. A. Cibula: *J. Inst. Met.*, 1949–1950, vol. 76, pp. 321–60.
2. F. Crossley and L. Mondolfo: *JOM*, 1951, vol. 191, pp. 1143–51.
3. B.S. Murty, S.A. Kori, and M. Chakraborty: *Int. Mater. Rev.*, 2002, vol. 47 (1), pp. 3–29.
4. M.A. Easton and D.H. StJohn: *Metall. Mater. Trans. A*, 2005, vol. 36A, pp. 1911–20.
5. A.L. Greer, A.M. Bunn, A. Tronche, P.V. Evans, and D.J. Bristow: *Acta Mater.*, 2000, vol. 48, pp. 2823–35.
6. T.E. Quested and A.L. Greer: *Acta Mater.*, 2004, vol. 52, pp. 3859–68.
7. M.A. Easton and D.H. StJohn: *Acta Mater.*, 2001, vol. 49 (10), pp. 1867–78.
8. C. Càceres and Q. Wang: *Int. J. Cast Met. Res.*, 1996, vol. 9 (3), pp. 157–62.
9. C.Y. Wang, S. Ahuja, C. Beckerman, and H.C. de Groh: *Metall. Mater. Trans. B*, 1995, vol. 26B, pp. 111–19.
10. Ø. Nielsen, L. Arnberg, A. Mo, and H. Thevik: *Metall. Mater. Trans. A*, 1999, vol. 30A, pp. 2455–62.
11. J.A. Spittle and S.G. Brown: *Mater. Sci. Technol.*, 2005, vol. 21 (9), pp. 1–7.
12. M.A. Easton, J.F. Grandfield, D.H. StJohn, and B. Rinderer: *Mater. Sci. Forum*, 2006, vols. 519–521, pp. 1675–80.
13. Y.Z. Zhou and A. Volek: *Scripta Mater.*, 2007, vol. 56, pp. 537–40.
14. W. Kurz and D. Fisher: *Fundamentals of Solidification*, 4th ed., Trans Tech Publications, Uetikon-Zurich, Switzerland, 1998.
15. M. Qian: *Acta Mater.*, 2006, vol. 54 (8), pp. 2241–52.
16. M. Qian, D.H. StJohn, and M.T. Frost: *Scripta Mater.*, 2002, vol. 46 (9), pp. 649–54.
17. M.A. Easton and D.H. StJohn: *Mater. Sci. Technol.*, 2000, vol. 16 (9), pp. 993–1000.
18. M. Johnsson: *Light Metals 1993*, TMS, Warrendale, PA, 1993, pp. 769–77.
19. M.C. Flemings, T.Z. Kattamis, and B.P. Bardes: *AFS Trans.*, 1991, vol. 99, pp. 501–06.
20. H.D. Brody and M.C. Flemings: *Trans. AIME*, 1966, vol. 236 (5), pp. 615–24.
21. H.-J. Diepers, C. Beckerman, and I. Steinbach: *Acta Mater.*, 1999, vol. 47 (13), pp. 3663–78.
22. A. Mortensen: *Metall. Trans. A*, 1991, vol. 22A, pp. 569–74.
23. M.E. Glicksman, R.N. Smith, S.P. Marsh, and R. Kuklinski: *Metall. Trans. A*, 1992, vol. 23A, pp. 659–67.
24. Z. Fan: *Int. Mater. Rev.*, 2002, vol. 47 (2), pp. 49–85.
25. A. Mortensen: *Metall. Trans. A*, 1989, vol. 20A, pp. 247–53.
26. M. Bamberger, B.Z. Weiss, and M.M. Stupel: *Mater. Sci. Technol.*, 1987, vol. 3, pp. 49–56.
27. K.P. Young and D.H. Kirkwood: *Metall. Trans. A*, 1975, vol. 6A, pp. 197–205.
28. L. Bäckerud, E. Król, and J. Tamminen: *Solidification Characteristics of Aluminium Alloys, Vol. 1: Wrought Alloys*, AFS/Skanaluminium, Oslo, 1993.
29. S. Blais, W. Loue, and C. Pluchon: *Proc. 4th Int. Conf. on Semi-solid Processing of Alloys and Composites,* The University of Sheffield, Sheffield, 1996, pp. 187–92.
30. M. Rappaz and W.J. Boettinger: *Acta Mater.*, 1999, vol. 47 (11), pp. 3205–19.
31. D.H. Kirkwood: *Mater. Sci. Eng.*, 1985, vol. 73, pp. L1–L4.
32. L. Ratke and W. Thieringer: *Acta Metall.*, 1985, vol. 33 (10), pp. 1793–1802.
33. S. Steinbach and L. Ratke: *Mater. Sci. Eng., A*, 2005, vols. 413–414, pp. 200–04.
34. U. Hecht, L. Gránásy, T. Pusztai, B. Böttger, M. Apel, V. Witusiewicz, L. Ratke, J.D. Wilde, L. Froyen, D. Camel, B. Drevet, G. Faivre, S.G. Fries, B. Legendre, and S. Rex: *Mater. Sci. Eng., R*, 2004, vol. 46 (1–2), pp. 1–49.
35. M. Ode, S.G. Kim, W.T. Kim, and T. Suzuki: *ISIJ Int.*, 2001, vol. 41 (4), pp. 345–49.
36. T. Suzuki, M. Ode, S.G. Kim, and W.T. Kim: *J. Cryst. Growth*, 2002, vols. 237–239 (part I), pp. 125–31.
37. P.-R. Cha, D.-H. Yeon, and J.-K. Yoon: *Acta Mater.*, 2001, vol. 49, pp. 3295–3307.
38. M.-F. Zhu, W. Cao, S.-L. Chen, C.-P. Hong, and Y.A. Chang: *J. Phase Equilib. Diff.*, 2007, vol. 28 (1), pp. 130–38.
39. P.N. Anyalebechi: *EPD Congress 2004*, TMS, Warrendale, PA, 2004, pp. 217–33.
40. V. Ronto and A. Roosz: *Int. J. Cast Met. Res.*, 2001, vol. 13 (6), pp. 337–42.
41. M.A. Easton and D.H. StJohn: *Light Metals 2001*, TMS, Warrendale, PA, 2001, pp. 927–34.
42. M.A. Easton and D.H. StJohn: *Mater. Sci. Eng., A*, 2008, vol. 486 (1–2), pp. 8–13.
43. L. Bäckerud, E. Król, and J. Tamminen: in *Solidification Characteristics of Aluminium Alloys Vol. 1*, L. Bäckerud, ed., Skanaluminium, Universitetsforlaget AS, Oslo, Norway, 1986, pp. 63–74.
44. R.E. Spear and G.R. Gardner: *Mod. Castings*, 1963, vol. 43 (5), pp. 209–15.
45. Ø. Nielsen, B. Appolaire, H. Combeau, and A. Mo: *Metall. Mater. Trans. A*, 2001, vol. 32A, pp. 2049–60.
46. M.W. Chase: *NIST-JANAF Thermochemical Tables*, 4th ed., American Institute of Physics, Melville, NY, 1998; *J. Phys. Chem. Ref. Data*, 1998, monograph no. 9.
47. M. Rappaz, A. Jacot, and W.J. Boettinger: *Metall. Mater. Trans. A*, 2003, vol. 34A, pp. 467–79.
48. M. Rappaz and P. Thévoz: *Acta Metall.*, 1987, vol. 35 (7), pp. 1487–97.
49. Y. Du, Y.A. Chang, B. Huang, W. Gong, Z. Jin, H. Xu, Z. Yuan, Y. Liu, Y. He, and F.-Y. Xie: *Mater. Sci. Eng., A*, 2003, vol. 363, pp. 140–51.
50. J. Kron, A. Lagerstdt, and H. Fredriksson: *Int. J. Cast Met. Res.*, 2004, vol. 18 (1), pp. 29–40.
51. O. Ludwig, M. Dimichiel, L. Salvo, M. Suéry, and P. Falus: *Metall. Mater. Trans. A*, 2005, vol. 36A, pp. 1515–23.
52. H. Miyahara and K. Ogi: *Mater. Trans.*, 2001, vol. 42 (2), pp. 252–57.
53. Z. Guo, N. Saunders, A.P. Miodownik, and J.P. Schillé: *Mater. Sci. Eng., A*, 2005, vols. 413–414, pp. 465–69.
54. N. Saunders, Z. Guo, X. Li, A.P. Miodownik, and J.P. Schille: *JOM*, 2003, vol. 55 (12), pp. 60–65.
55. I. Maxwell and A. Hellawell: *Acta Metall.*, 1975, vol. 23, pp. 229–37.
56. M. Johnsson: *Z. Metallkd.*, 1994, vol. 85, pp. 781–85.
57. M. Johnsson and L. Bäckerud: *Z. Metallkd.*, 1996, vol. 87 (3), pp. 216–20.
58. D.G. McCartney: *Int. Mater. Rev.*, 1989, vol. 34, pp. 247–60.